4. RESULTS AND DISCUSSION

4.1 Charactrization of the organomodified bentonite (OBTN), Porous Clay Heterostructure (PCH) and Functionalized Porous Clay Heterostructure (APPCH)

The sodium bentonite clay (Na-BTN) and the obtained modified clay (OBTN, PCH and APPCH) were shown in Figure 4.1.

(a) (b) (c) (d)

Figure 4.1 (a) Na-BTN, (b) OBTN, (c) PCH and (d) APPCH.

The organomodified bentonite (OBTN) was confirmed the expansion of sodium bentonite (Na-BTN) layers by incorporating of cationic surfactant and studied the effect of using different surfactant by XRD. Figure 4.2 showed XRD results of Na-BTN and OBTN. The XRD pattern showed the presence of the (001) reflection peak. The d_{001} peak of Na-BTN at $2\theta = 7.10°$ which corresponded to the basal spacing of 1.24 nm (Figure 4.2 a). After modified Na-BTN with cationic surfactant, cetyl trimethyl ammonium bromide (CTAB), OBTN showed the d_{001} peak at lower angle of 2.25° which corresponded to the basal spacing of 3.93 nm (Figure 4.2 b) indicating the increasing the basal spacing of clay layers due to ammonium ions from cationic surfactant intercalated into the silicate layers. In addition, the XRD result showed that the obtained OBTN synthesized from the surfactant, cetyl

trimethyl ammonium chloride (CTAC) as shown in Figure 4.2 c showed the increasing the basal spacing of clay layers but the d-spacing less than the OBTN synthesized from CTAB [1].

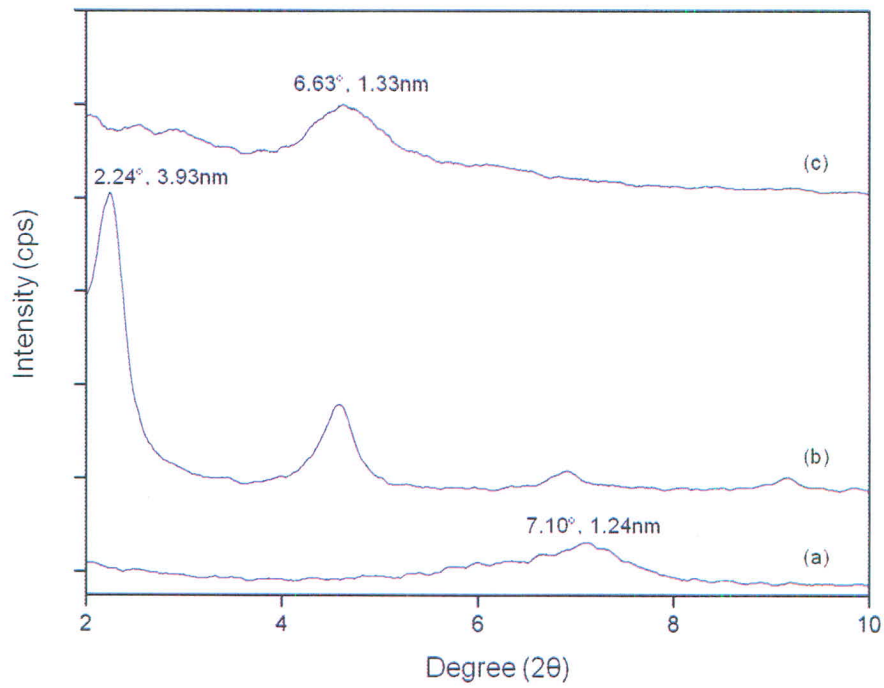

Figure 4.2 The XRD patterns of (a) Na-BTN, (b) OBTN (CTAB) and (c) OBTN (CTAC).

From the FTIR results (Figure 4.3), the FTIR spectrum of Na-BTN (Figure 4.3 a) showed the peak at around 3500 cm^{-1} assigned to the stretching vibration of the silanol associated with the silica structure and the peak at around 1000 cm^{-1} assigned to the stretching vibration of the SiO_4 units. The peaks at around 1100 and 800 cm^{-1} were assigned to the asymmetric and symmetric stretching vibrations of the Si-O-Si linkage. The presence of surfactant in the layer of BTN was indicated by FTIR spectra of OBTN (Figure 4.3 b). The peaks at 2919 and 2850 cm^{-1} were assigned to asymmetric and symmetric stretching vibrations of methyl and methylene groups of hexadecyltrimethylammonium ion respectively. The FTIR spectra of PCH (Figure 4.3 c) and APPCH (Figure 4.3 d) were different from Na-BTN at the absence of the peak at 1000 cm^{-1} because of the changing of clay structure after modification.

In addition, the peak at around 1510 cm^{-1} were confirmed the organic group ($-NH_2$) from APTES molecule in the structure of APPCH [2].

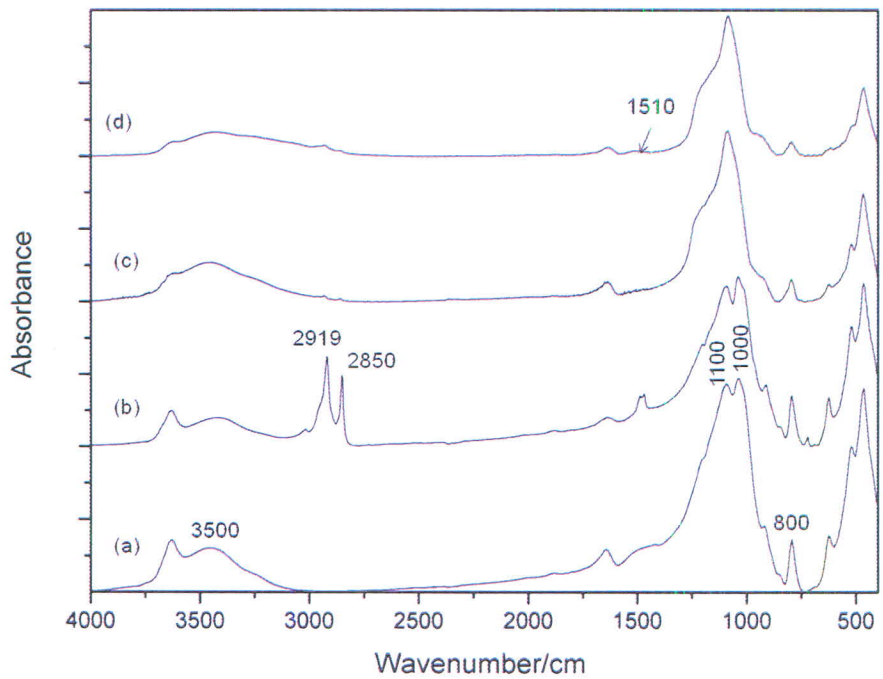

Figure 4.3 Fourier transform infrared spectroscopy spectra of (a) Na-BTN, (b) OBTN, (c) PCH and (d) APPCH.

The morphology of Na-BTN and modified clay were characterized by SEM image. The flat plate structure of Na-BTN was observed (Figure 4.4 a). After porous samples were synthesized within the galleries of bentonite by the polymerization of tetraethoxysilane (TEOS) in the presence of surfactant micelles, the rugged surface of PCH (Figure 4.4 b) and APPCH (Figure 4.4 c) were presented because of the formation of pore structure in the galleries of clay [3].

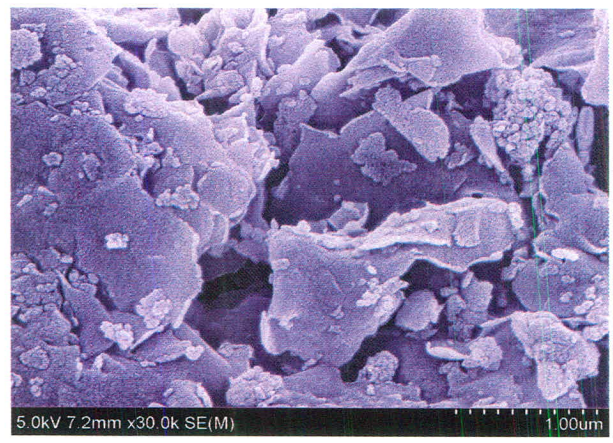

(a)

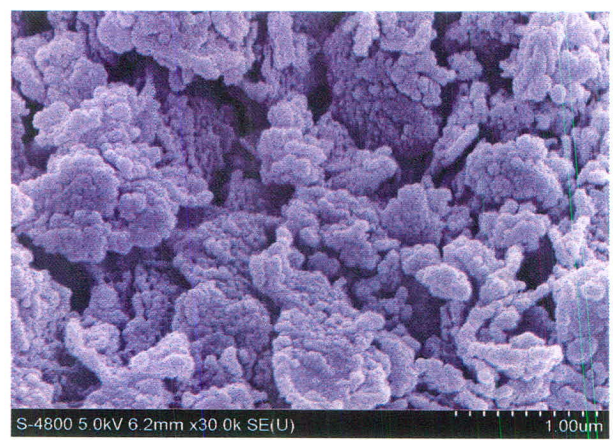

(b)

Figure 4.4 Scanning electron microscope images of (a) Na-BTN, (b) PCH.

The results from nitrogen adsorption-desorption (Table 4.1) showed the increasing of specific surface area of porous material (PCH and APPCH) compared with Na-BTN. The results revealed that PCH had the high surface areas of 524.1 m^2/g, average pore diameter of 4.85 nm and pore volume of 0.64 cc/g. While the functionalized PCH (APPCH) with amino group ($-NH_2$) had the decrease of surface area and pore volume compared to PCH and the increasing of APTES content reduced surface area and pore volume. The values of surface area and pore volume were in the range of 119.8-320.5 m^2/g and 0.33-0.42 cc/g, respectively. The results indicated that the incorporation of amino group ($-NH_2$) in porous structure was successful [3, 4, 5].

Table 4.1 Surface area, pore diameters and pore volume from nitrogen adsorption-desorption

Sample	Multipoint BET surface area (m^2/g)	Average pore diameter (nm)	Pore volume (cc/g)
Na-BTN	31.0	-	-
PCH	524.1	4.85	0.64

4.2 Characterization of Chromophores Modified PCH

The morphology of the chromophores (bromothymol blue) modified PCH, was determined by nitrogen adsorption-desorption and the results were reported in Table 4.4. The results showed that the surface area and pore volume of PCH decreased while the average pore diameter increased after modification the porous sample with pH dye. The chromophores modified PCH (PCH-BTB) had the surface area of 32-57 m^2/g, average pore diameter in range of 20.12-25.77 nm and pore volume of 0.21-0.29 cc/g. The large decrease of surface area and increase of average pore diameter of PCH after modification with pH dye indicated that the large molecule of bromothymol blue incorporated into the structure of PCH and the amount of dye content not have the influence to decrease the surface area.

The chromophores (bromothymol blue) modified PCH were prepared as shown in Figure 4.5.

Table 4.2 Surface area, pore diameters and pore volume from nitrogen adsorption-desorption

Sample	Multipoint BET surface area (m^2/g)	Average pore diameter (nm)	Pore volume (cc/g)
PCH	524.1	4.85	0.64
PCH-BTB (10:1)	37.73	23.65	0.22
PCH-BTB (20:1)	57.21	20.12	0.29
PCH-BTB (30:1)	32.94	25.77	0.21

10:1 20:1 30:1

Figure 4.5 Bromothymol blue modified PCH at various weight ratio of clay and pH dye; 10:1, 20:1 and 30:1.

The XRD patterns of the PCH and chromophores modified PCH (PCH-BTB) was shown in Figure 4.6 (a) – (d). The results showed that there was no obvious peak observed in XRD patterns of PCH. While the XRD patterns of PCH-BTB showed the peaks around 2θ = 6.6 nm which corresponded to the basal spacing about 1.3 nm might be due to the formation of the partial layer structure of PCH after modified with bromothymol blue.

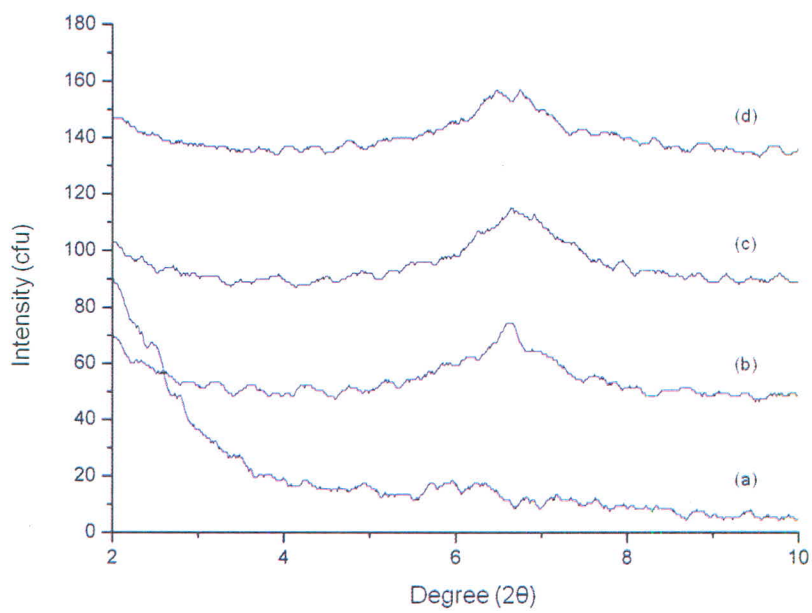

Figure 4.6 The XRD patterns of (a) PCH, (b) PCH-BTB 10:1, (c) PCH-BTB 20:1 and (d) PCH-BTB 30:1

The results of SEM image as shown in Figure 4.7 indicated that the rugged surface of PCH after modified with chromophore (bromothymol blue) still remained.

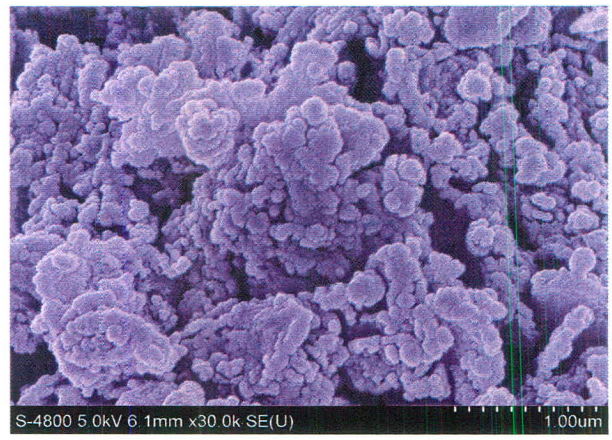

(a)

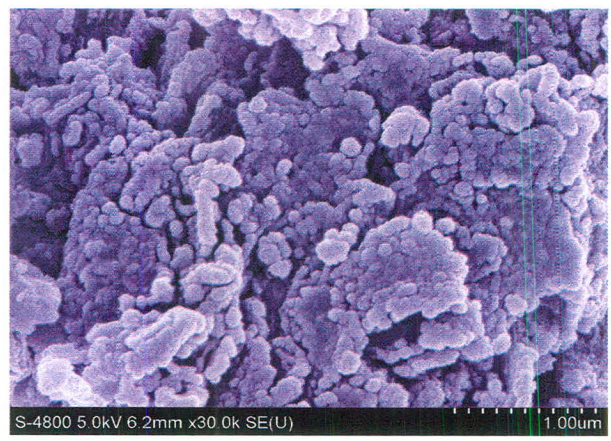

(b)

(c)

Figure 4.7 SEM images of (a) PCH-BTB 10:1, (b) PCH-BTB 20:1 and (c) PCH-BTB 30:1.

4.3 pH Indicator Film Response to Standard CO_2 and H_2O

Because the ripening of climacteric fruit associates with increasing in respiration and the main products from respiration of climacteric fruits such as carbon dioxide and water are generally to measure. Thus, carbon dioxide and water releasing before climacteric peak at the time that the fruit starts to ripen is the most important parameter to evaluate the freshness of the climacteric fruit by the color change of pH indicator films [3].

The color change of indicator films (LDPE/PCH-BTB nanocomposite films) after test with excess water and standard carbon dioxide (CO_2) at concentration from 0 to 150 ppm which can be compared with the production of CO_2 in the preclimacteric to climacteric phase during fruit ripening was shown in Table 4.3, Table 4.4, Table 4.5 and Figure 4.8. The result showed that the color of indicator film changed the color from green to yellow correlated with increasing in standard CO_2 levels as shown in Figure 4.9. The total color difference (ΔE) and hunter b values continuously increases at low concentration of standard CO_2 and remaining constant at high concentrations due to the saturation of color change. Moreover, the pH indicator film PCH-BTB 10:1 showed the highest sensitivity of color change compared to PCH-BTB 20:1 and PCH-BTB 30:1 at low concentrations of standard CO_2. The reaction of color change was described. Carbon dioxide combined with water and producing carbonic acid. Carbonic acid dissociated from parent molecule forming hydrogen ions (H^+) and bicarbonate ion (HCO^{3-}). Then, as a proton, a hydrogen ion combined with water molecule to form a hydronium ion (H_3O^+). Hydronium ions reacted with the bromothymol blue in basic form resulting in an acid form. The color change of indicator film was presented. The mechanism of color change was shown in Figure 2.7. Therefore, this pH indicator film can be applied for detecting the quality of climacteric fruit by color change.

Table 4.3 Change in hunter color (L, a, b) and total color difference (TCD) values of LDPE/PCH-BTB (10:1) nanocomposite films after indirect contact with standard carbon dioxide and excess water

Concentration (ppm)	L	a	b	ΔL	Δa	Δb	ΔE
30	29.83	-5.45	3.03	-1.06	0.27	0.65	1.19
60	29.28	-6.61	3.75	0.52	0.5	1.53	1.69
90	28.42	-5.83	2.92	0.35	0.36	2.25	2.31
120	28.56	-5.48	2.86	0.79	0.47	2.00	2.20
150	29.05	-5.28	2.40	0.03	0.63	2.08	2.17

Table 4.4 Change in hunter color (L, a, b) and total color difference (TCD) values of LDPE/PCH-BTB (20:1) nanocomposite films after indirect contact with standard carbon dioxide and excess water

Concentration (ppm)	L	a	b	ΔL	Δa	Δb	ΔE
30	32.75	-6.73	1.42	0.55	0.32	0.30	0.70
60	32.28	-5.65	1.06	0.15	0.33	1.18	1.23
90	32.41	-5.78	1.08	-0.21	0.16	1.54	1.56
120	31.69	-6.08	0.62	0.36	0.56	2.01	2.12
150	32.23	-5.62	0.70	-0.12	0.32	2.15	2.18

Table 4.5 Change in hunter color (L, a, b) and total color difference (TCD) values of LDPE/PCH-BTB (30:1) nanocomposite films after indirect contact with standard carbon dioxide and excess water

Concentration (ppm)	L	a	b	ΔL	Δa	Δb	ΔE
30	32.53	-5.87	1.64	-0.02	0.08	0.33	0.35
60	31.27	-5.39	0.70	-0.04	0.17	1.23	1.24
90	33.37	-5.97	1.18	-1.18	-0.17	2.05	2.37
120	33.15	-5.80	1.10	0.50	0.09	2.24	2.49
150	31.19	-5.70	0.78	0.16	0.16	2.23	2.24

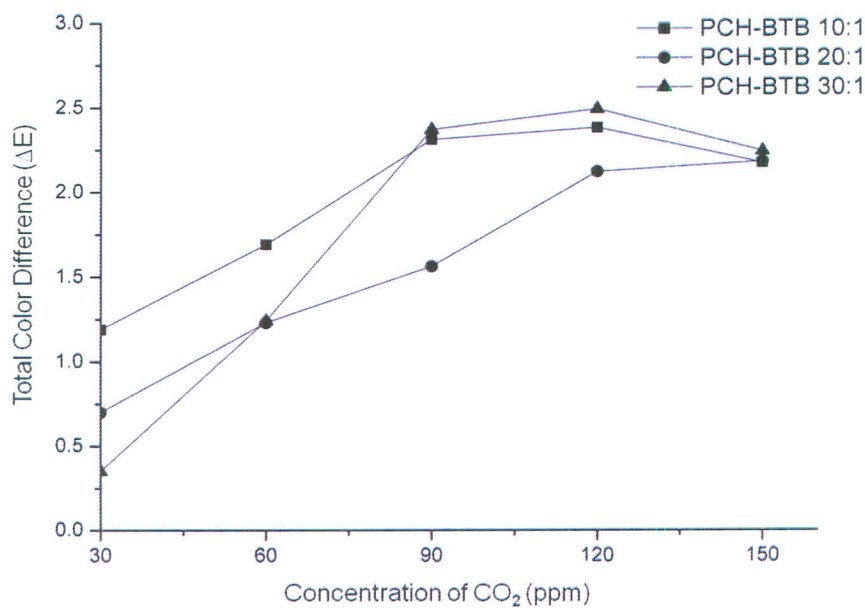

Figure 4.8 Changes in total color difference values (ΔE) of pH indicator film at various weight ratio of PCH: BTB (a) 10:1 (b) 20:1 and (c) 30:1.

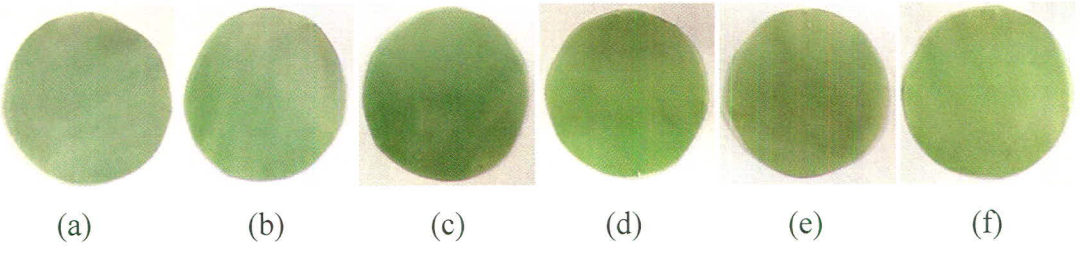

(a) (b) (c) (d) (e) (f)

Figure 4.9 Color changes of LDPE/PCH-BTB (10:1) nanocomposite films after test with standard carbon dioxide at various concentrations (a) 0 ppm (b) 30 ppm (c) 60 ppm (d) 90 ppm (e) 120 ppm and (f) 150 ppm.

4.4 pH Indicator Film Response to Fresh Banana

The result of indicator film response after in direct contact with fresh banana was observed. The pH change during storage was shown in Figure 4.10. The result showed that the color of indicator film changed the color from green to yellow when banana started to ripen and remained constant due to the saturation of color as shown in Figure 4.11 and 4.12.

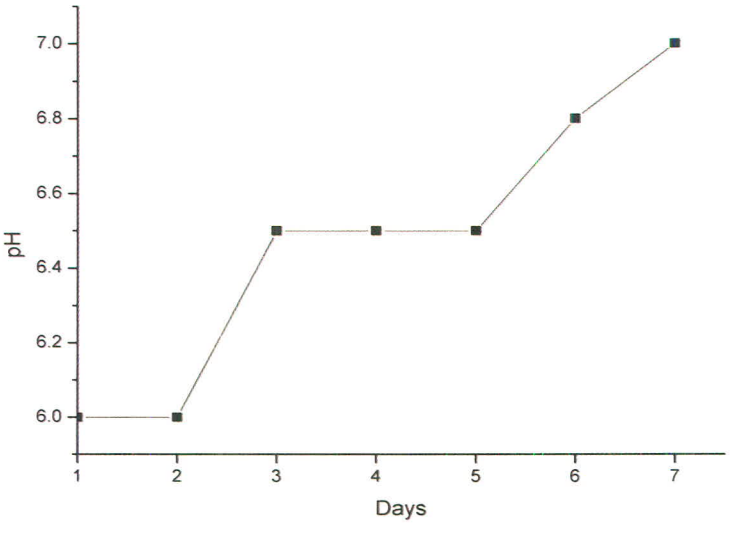

Figure 4.10 Changes in pH of fresh banana during storage at room temperature.

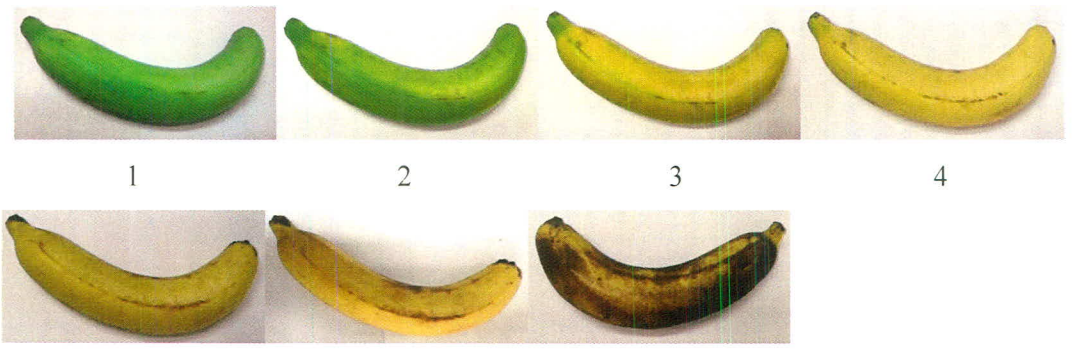

Figure 4.11 Reference bananas ripening at room temperature.

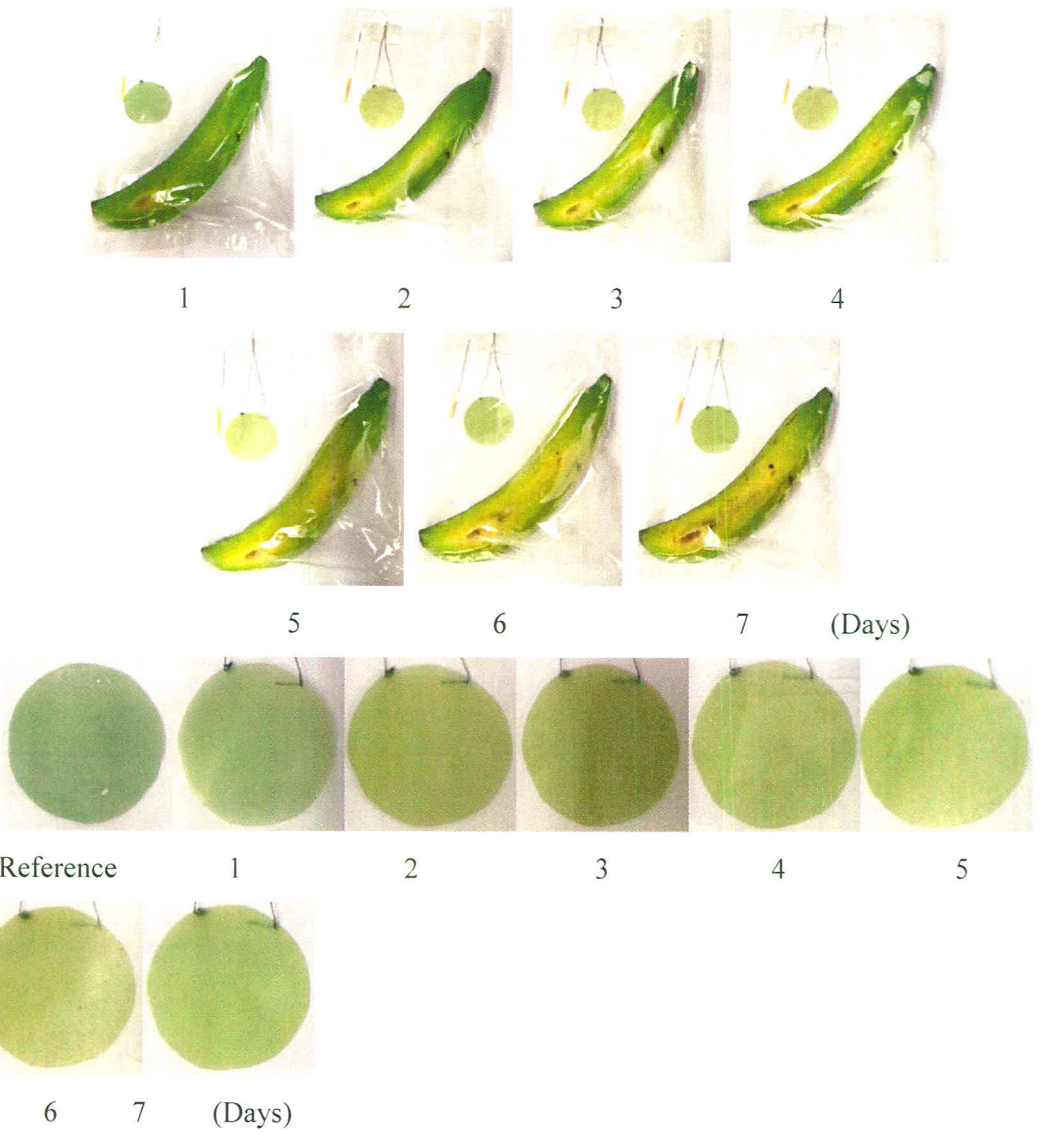

Figure 4.12 Color change of LDPE/PCH-BTB (10:1) nanocomposite film during banana ripening.

4.5 Leaching Studies

The leakage of the indicator dyes from the LDPE/PCH-BTB nanocomposite films with calibration curves was observed by UV-Vis spectrometer as shown in Figure 4.14, respectively. After the both indicator films were soaked in water and carried out to detect the presence of pH dye. The results showed that the absorbance of water was about zero equaled to the absorbance of reference distill water. Thus, the results indicated that no have leakage of bromothymol blue from both pH indicator films.

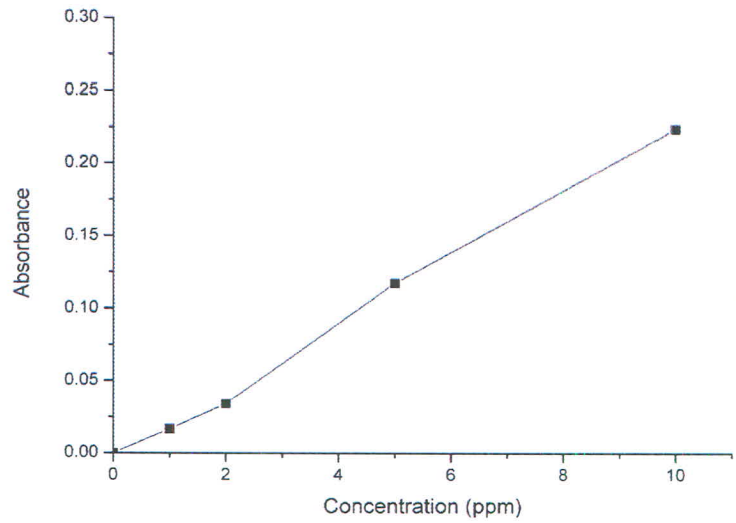

Figure 4.13 The leakage of bromothymol blue from LDPE/PCH-BTB nanocomposite films

4.6 Thermal Behavior of Nanocomposites

The crystallization temperature and melting temperature were measured by DSC. The result showed that the crystallization temperature of LDPE/PCH-BTB nanocomposites remained constant. The melting temperature of LDPE/PCH-BTB nanocomposites closed to neat LDPE. Moreover, the results indicated that the crystalline and melting characteristics of nanocomposites were not dependent on dye content. DSC thermograms of nanocomposites are shown in Figure 4.15.

The thermal degradation temperature was measured by TGA. TG-DTA curves were shown in Figure 4.16. The results showed that the thermal degradation occurred in single stage. The nanocomposites showed the higher thermal stability than neat LDPE. This behavior may be attributed to the formation of a high-performance carbonaceous silicate char build up on the surface [2].

Melting, crystallization and thermal behavior results are shown in Table 4.6 and 4.7.

Table 4.6 Melting and crystallization behavior

Sample	T_C (°C)	T_m (°C)	ΔH_m (J/g)	%Crystallinity
LDPE	95.01	109.10	69.58	33.29
LDPE/6%wtSurlyn	95.22	109.31	76.67	36.68
LDPE/6%wtSurlyn/2%wtPCH-BTB(10:1)	95.78	108.76	70.52	33.74
LDPE/6%wtSurlyn/2%wtPCH-BTB(20:1)	95.28	109.27	71.46	34.19
LDPE/6%wtSurlyn/2%wtPCH-BTB(30:1)	95.57	109.29	71.08	34.01

Table 4.7 Thermal behavior

Sample	Char residue (%wt)	T_d (°C)
LDPE	1.2	449.0
LDPE/6%wtSurlyn	0.2	450.7
LDPE/6%wtSurlyn/2%wtPCH-BTB(10:1)	2.9	451.9
LDPE/6%wtSurlyn/2%wtPCH-BTB(20:1)	5.0	449.0
LDPE/6%wtSurlyn/2%wtPCH-BTB(30:1)	2.6	453.0

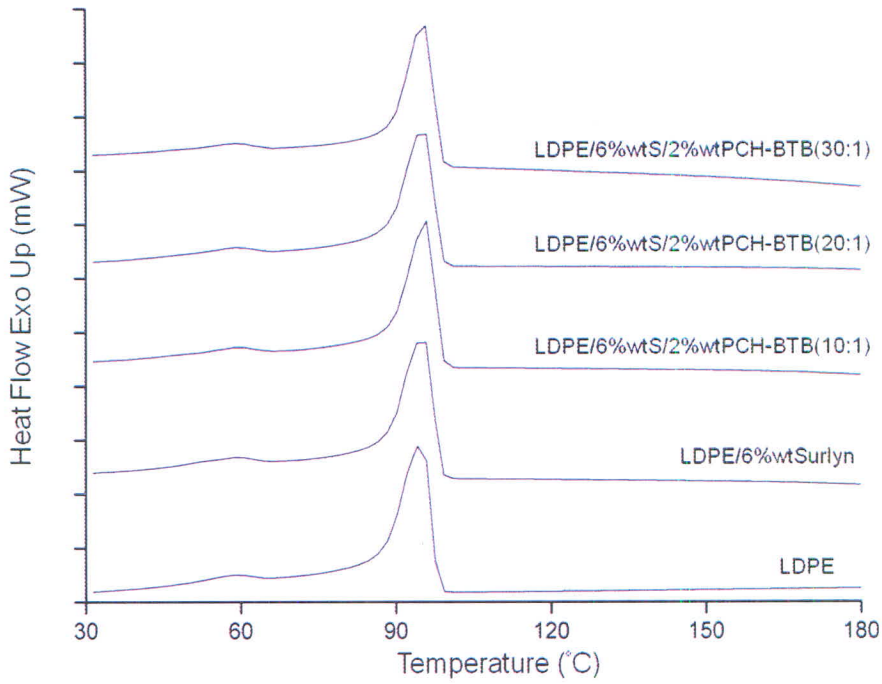

(a)

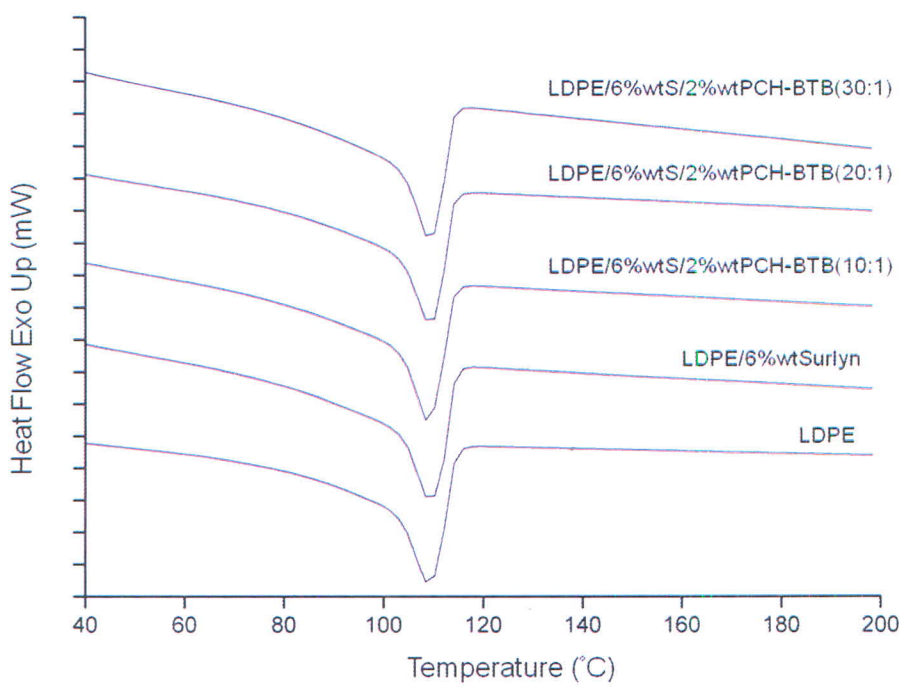

(b)

Figure 4.14 DSC thermograms of LDPE/PCH-BTB nanocomposites (a) crystallization temperature and (b) melting temperature.

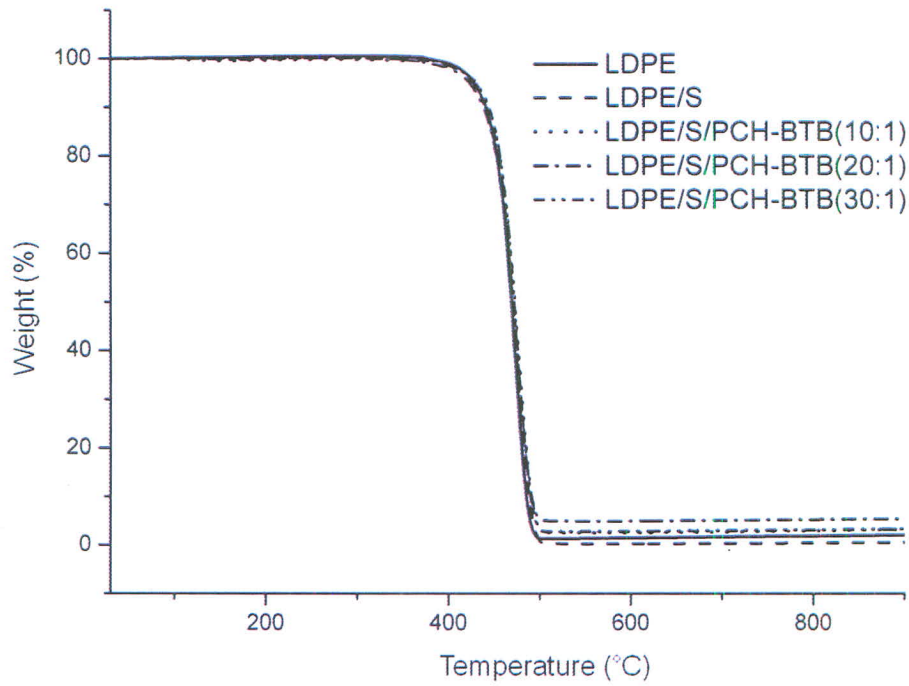

Figure 4.15 TG curves of LDPE/PCH-BTB nanocomposites

4.7 Mechanical Properties of Nanocomposites

The mechanical properties of LDPE/PCH-BTB nanocomposite films compared to neat LDPE were shown in Figure 4.17, 4.18 and 4.19. The result showed that Young's modulus and tensile strength increased in the presence of clay in nanocomposite films due to the porous clay acting as the excellent filler with enable to reinforce the films. While % elongation at yield decreased in the presence of clay in nanocomposite films. The possible reason may be due to the addition of clay was attributed to increase stiffness of polymer [6].

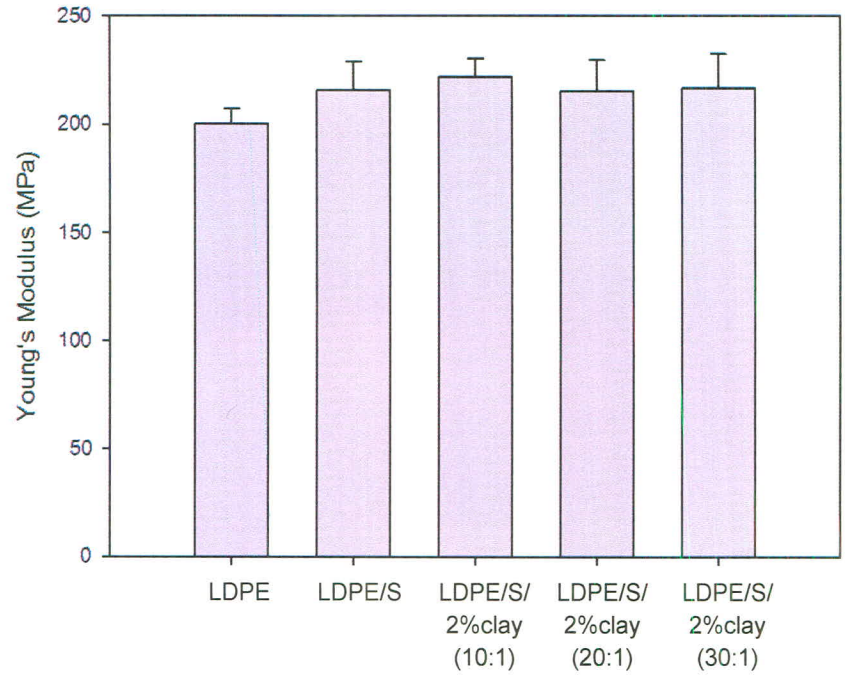

Figure 4.16 Young's modulus of LDPE and LDPE/PCH-BTB nanocomposite films.

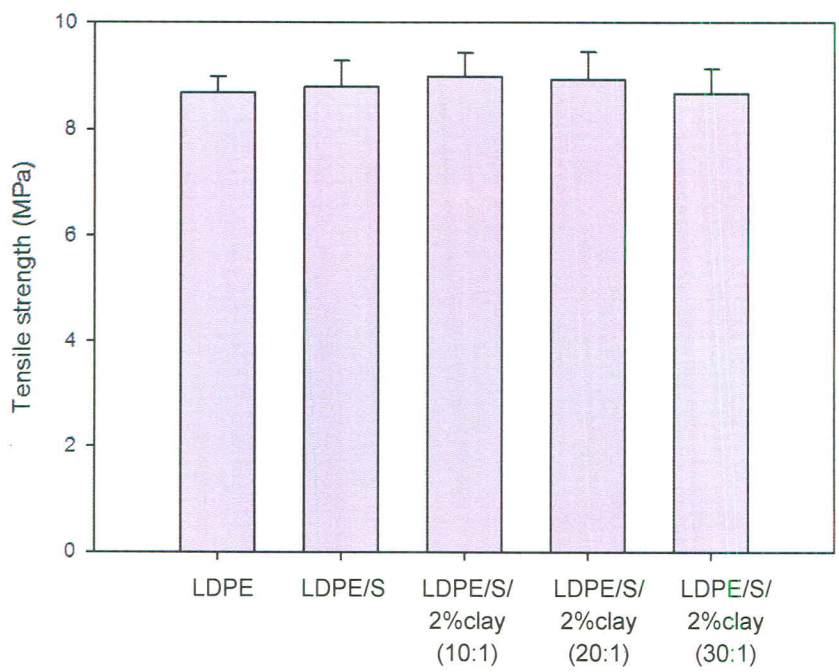

Figure 4.17 Tensile strength of LDPE and LDPE/PCH-BTB nanocomposite films.

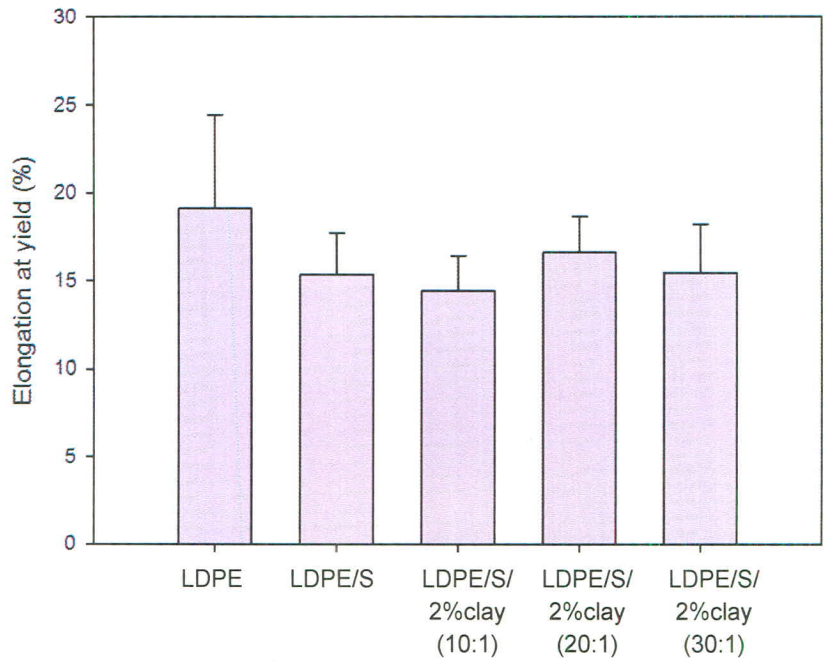

Figure 4.18 % Elongation at yield of LDPE and LDPE/PCH-BTB nanocomposite films.

4.8 Oxygen Gas Permeability of Nanocomposite Films

Oxygen gas transmission rate of nanocomposites was shown in Table 4.8. The results showed the reduction of oxygen transmission rate in nanocomposites compared to neat LDPE. Porous clay improved the barrier properties of nanocomposite indicated by the reduction of oxygen transmission rate in the nanocomposites. The improvement in barrier properties of nanocomposites was due to the presence of porous clay which provided the tortuous path in polymer matrix.

Table 4.8 Oxygen gas transmission rate of LDPE and LDPE/PCH-BTB nanocomposites

Sample	Oxygen gas transmission rate ($cc/m^2.day$)
LDPE	257
LDPE/PCH-BTB (10:1)	225
LDPE/PCH-BTB (30:1)	230